

some part overflows at the first quadrant, which also does not reach the chute. Low discharge efficiency results in both cases.

In the case of centrifugal discharge most particles are interrupted in the free motion by the bucket's front wall and flows out near the bucket edge. The motion of these particles after leaving the bucket can be estimated approximately by

assuming that any particle starts from the bucket edge with an initial velocity equal to the circumferential velocity of that point.

This work was subsidized by the Scientific Research Fund of the Ministry of Education.

### Reference

- (1) C.V. Hanffstengel: *Die Förderung von Massengütern* 1, 3 Aufl. (1921), S. 130.

621.67:539.528

## Experimental Study on Cavitation in Centrifugal Pump Impellers\*

By Shungo MINAMI\*\*, Kyoji KAWAGUCHI\*\*\*,  
and Tetsuo HOMMA\*\*\*

Investigations concerning cavitation in several impellers with three dimensional blades were carried out using a 200 mm bore single suction pump installed in a closed circuit system. Flow inside the impeller was observed with strobo-light, and the NPSH at the condition of cavitation incipience measured for each impeller was found to show a peculiar variation against capacity taking a minimum at or near the designed flow rate and a peak at a partial capacity. The flow at the impeller inlet was measured with a Pitot tube and it was clarified that the flow pattern which accompanied remarkable swirling and back flow at partial capacities was responsible for the above NPSH variation. The cavitation aspects in the impellers are presented by photographs and their correlations with the various local pressure drops are discussed. The impellers were compared in terms of pressure drop coefficients as well as the suction specific speed plotted versus capacities with a view to applying them to the practical fields.

### 1. Introduction

The cavitation phenomenon is one of the most important problems to be considered sufficiently in designing and operating a pump. Especially when the speed-up of pumps is highly demanded as is today, its importance becomes greater. However, experimental researches as well as theoretical studies<sup>(1)(2)</sup> are required in the field of centrifugal pumps, in order to clarify the complicated aspects of cavitation which appear in impellers as well as to improve their suction characteristics. In this treatise, the results of experiments conducted on cavitation in several kinds of three dimensional

impellers are presented as follows:

### 2. Experimental methods and test impellers

The testing pump employed was a single suction volute pump of 200 mm in suction bore; its sectional view is shown in Fig. 1. The front shroud of the impeller, a part of the suction cover, as well as a part of the suction pipe were made of transparent plastic material in order to observe the cavitation phenomena by strobo-light. A 30 HP, 6-pole induction motor was used for the pump drive, its synchronous speed being 1000 r. p. m. As shown in Fig. 2, the test apparatus was a closed circuit system applying a vacuum tank of approximately 6 cubic meter capacity. Water flowed from the tank via a rectification lattice, a converging pipe, and a straight pipe into the test pump.

\* Received 3rd February, 1959.

\*\* Vice-Chief, Design Department, Ebara Manufacturing Co. Ltd., Ota-ku, Tokyo.

\*\*\* Design Department, Ebara Manufacturing Co. Ltd.

Water on the delivery side flowed through the orifice for measuring the flow rate, and through a sluice valve for controlling the pump capacity, and circulated to the opposite side of the tank. A partition plate was provided inside the tank to prevent bubbles formed in water from recirculating into the suction pipe. In order to control the suction pressure at will, pipings were fixed on the top of the tank, and connected with 2 units of the Nash type vacuum pump arranged in series. The water temperature in the circuit during the tests was in the range from 10 to 28°C, and water supplied by city waterworks was used.

At first, in cavitation tests, the change of Net

Positive Suction Head (NPSH) which gave incipience of cavitation at the impeller was measured over a wide range of capacity by observing with strobo-light. Secondly, keeping NPSH constant, the change of pump characteristics due to cavitation was measured against capacity. Growth of cavitation was also observed together with the above tests. In order to avoid the influence of vortex motion at the impeller eye on the suction pressure at partial capacities, an U-tube mercury manometer was placed apart approximately 8 times the pipe dia. from the pump inlet (See the point  $H_s$  in Fig. 2). The actual suction head was determined by taking into consideration the head

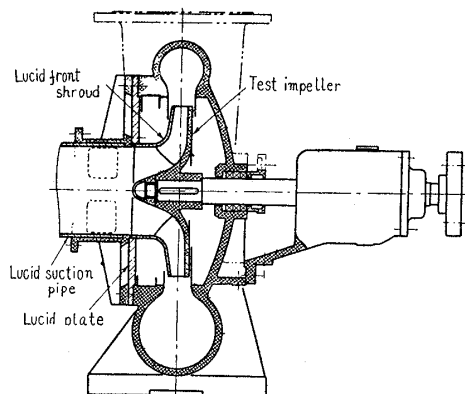


Fig. 1 Sectional view of test pump

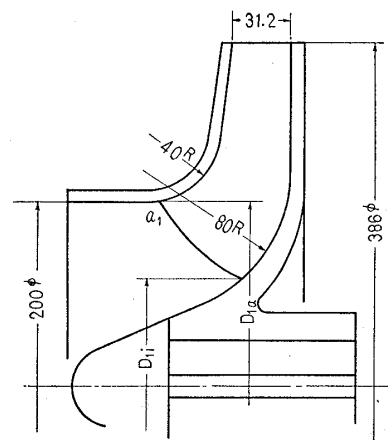


Fig. 3 Sectional view of test impellers

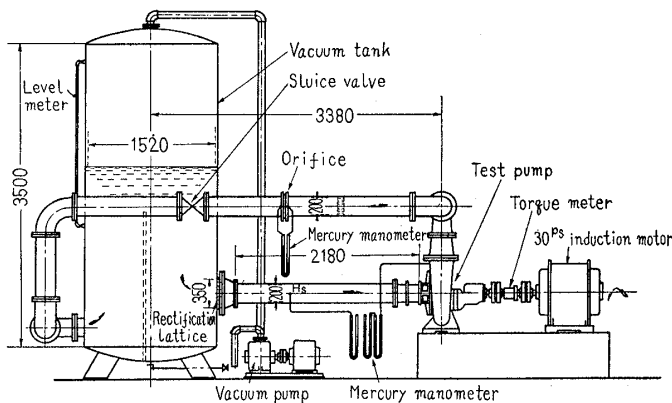
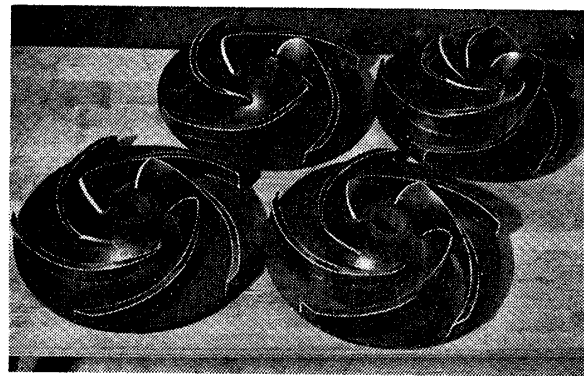


Fig. 2 Test circuit



(From right to left A-, B-, C-, and D-impellers)

Fig. 4 Test impellers with shroud removed

Table 1 Dimensions of test impellers

Item Impeller	Outside dia.	Outlet breadth	Outlet angle	Inlet dia. at periphe- ry side	Inlet dia. at hub side	Inlet angle at periphe- ry side	Inlet angle at hub side	Number of blades $Z$	Blade inlet area	Blade thick- ness at outlet	Blade thick- ness at inlet	Specific speed at max. efficiency point $n_s (\frac{m^3/min}{m, r.p.m.})$
	$D_2$ mm	$b_2$ mm	$\beta_2$	$D_{1a}$ mm	$D_{1i}$ mm	$\beta_{1a}$	$\beta_{1i}$		$A_0$ m	$S_2$ mm	$S_1$ mm	
A-Impeller	386	31.2	23°	201	115	22°20'	36°10'	5	0.028 0	12	6	350
B-Impeller	386	31.2	23°	201	115	22°20'	36°10'	4	0.028 0	12	6	386
C-Impeller	386	31.2	23°	202	115	21°50'	36°10'	5	0.028 0	12	3	350
D-Impeller	386	31.2	23°	200	78	22°40'	44°40'	5	0.030 2	12	4.5	368

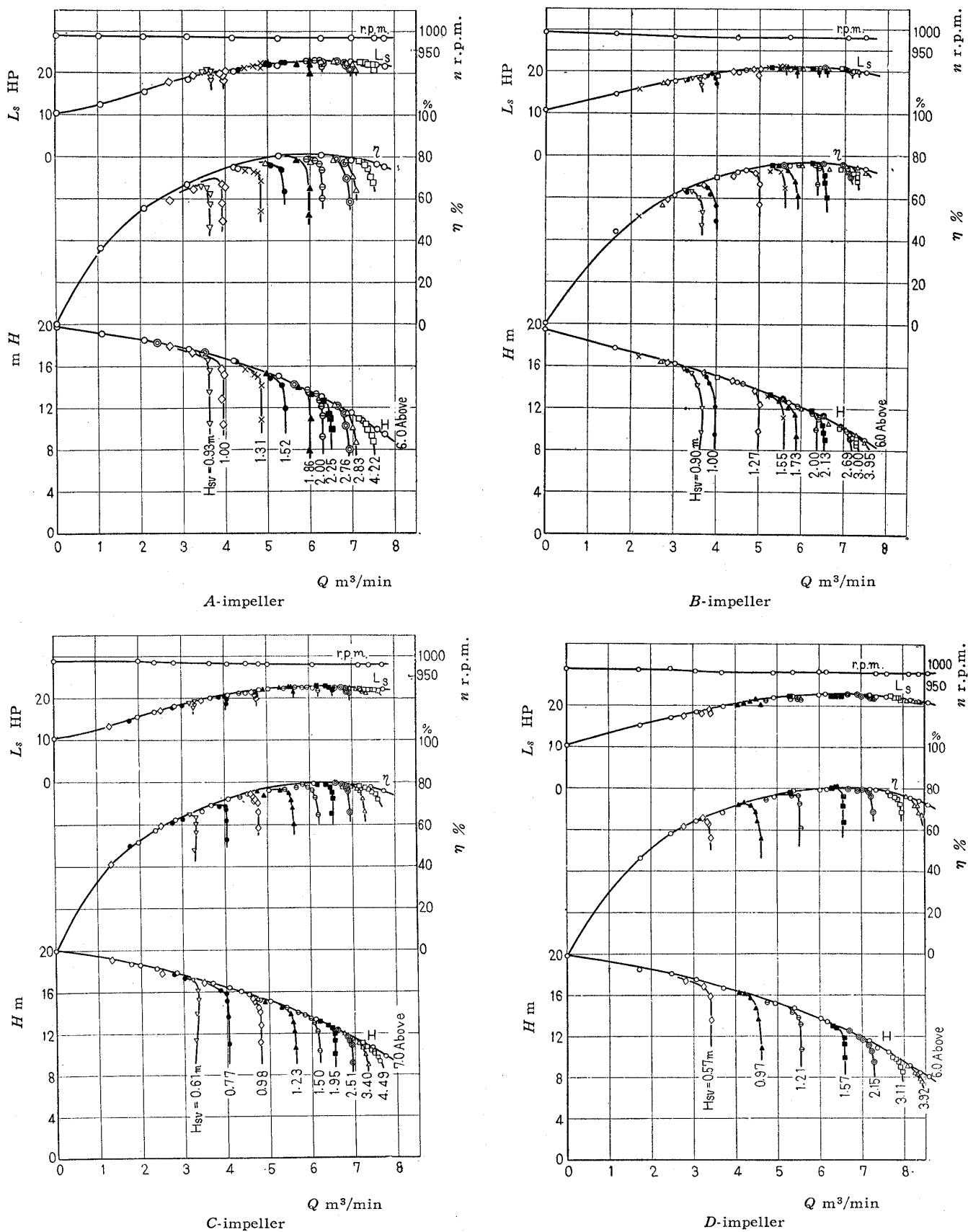


Fig. 5 Pump characteristics affected by cavitation



and efficiency  $\eta$  against capacity  $Q$  are plotted. Generally speaking, if capacity is increased under a certain value of NPSH, head deviates and drops from the standard  $H$ - $Q$  curve which is not attended with cavitation. And by further increase in the sluice valve opening, the capacity reaches a limit and the head drops straight downward, as was proved by many experiments<sup>(3)</sup>. The shaft horse power shows a slight increase near the point of the head drop, but it decreases with a further drop in the head. The efficiency variation shows a similar property to that of the head. From these results of experiments assuming  $H_{svd}$  as NPSH at the point at which the head curve deviates from the standard curve owing to the growth of cavitation, and  $H_{svi}$  as NPSH when the head curve drops straight downward, the relations between these two values ( $H_{svd}$  and  $H_{svi}$ ) and the capacity were studied. See Fig. 6 (a) to (d) in which all values were converted into 960 r. p. m. base. The curves show increases with the capacity approximately in a parabola; however, when the capacity exceeds the design point, the rate of increase generally becomes large.

The above mentioned is the change observed in the performance. However, by the observation of flow in the impeller, NPSH at the condition of visible incipience of cavitation assumed as  $H_{svi}$  was obtained, and its changes are also shown in Fig. 6. In general, incipient cavitation occurred at the point  $a_1$  in Fig. 3, where the peripheral velocity was maximum, and it hardly occurred at normal capacity and by further increase of flow the cavitation was apt to occur at the front side of impeller blades. (see Fig. 7) When the flow rate was small, cavitation appeared at the back side, and by further decrease of capacity the cavitating point moved inward from the  $a_1$  point of the blade backside towards the hub. With each impeller the NPSH at incipient cavitation shows a similar change. Generally, in the vicinity of designed flow rate  $H_{svi}$  is small and close to  $H_{svd}$ , showing that soon after this incipience the variation in pump characteristics is manifested. In this study the leakage at the impeller is presumed to be approximately 1%, therefore, it was omitted from calculation.

#### 4. Relations between flow conditions at the impeller inlet and incipience of cavitation

In order to clarify the relations between flow conditions and incipience of cavitation, a velocity triangle as shown in Fig. 7 will be taken into consideration. Now, assuming the inlet blade angle

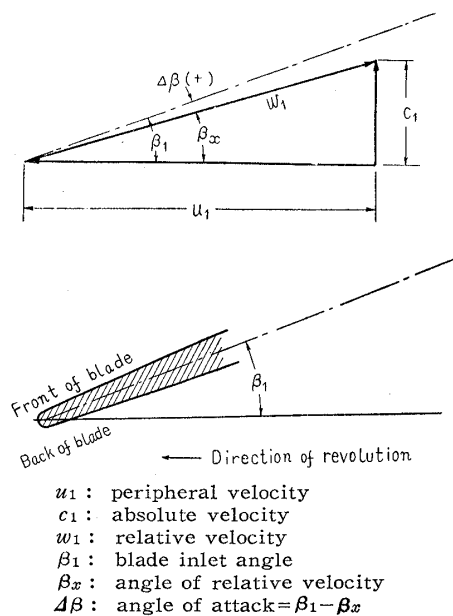


Fig. 7 Velocity triangle at blade inlet

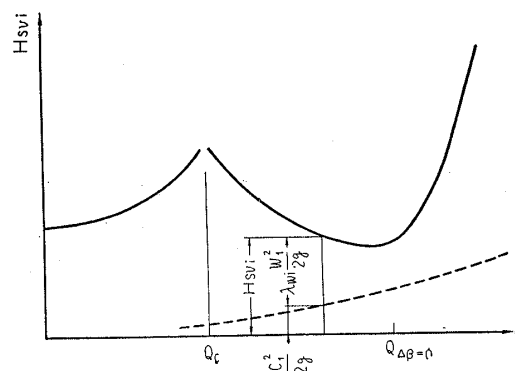


Fig. 8 Capacity versus NPSH at incipient condition

as  $\beta_1$ ,  $\beta_x$  denotes the direction of relative velocity at the blade inlet, calculated by assuming the inlet absolute velocity has no tangential component, and  $\Delta\beta$  denotes the angle between  $\beta_1$  and  $\beta_x$ . Regarding each impeller, the relation between the capacity and  $\Delta\beta$  estimated at the  $a_1$  point of Fig. 3 was obtained, and it was plotted along the capacity base in Fig. 6. As seen in each Figure, NPSH corresponding to the incipient cavitation at or about  $\Delta\beta = 0^\circ \sim 2^\circ$  shows minimum, and increases at both sides. This phenomenon will easily be presumed from the fact that if the angle of attack is large the pressure drop on the leading edge will increase and cavitation may occur<sup>(4)</sup>. Now, assuming the amount of pressure drop at the blade leading edge as  $\lambda_{wi}(w_1^2/2g)$  (where  $\lambda_{wi}$  is a coefficient of pressure drop), NPSH at incipient point will be expressed as follows :

$$H_{svi} = \frac{c_1^2}{2g} + \lambda_{wi} \frac{w_1^2}{2g} \dots\dots\dots (2)$$

As  $\lambda_{wi}$  shows minimum at  $\Delta\beta=0$ , and increases at its both sides (this will be shown later), Formula (2) will be converted to Fig.8 in respect of capacity. Then it is considered that  $H_{svi}$  shows minimum at a slightly smaller capacity than  $\Delta\beta=0$ .

When capacity was decreased and  $\Delta\beta$  was increased, in each impeller,  $H_{svi}$  showed the maximum value at a certain critical capacity  $Q_c$ , and when capacity became further small, the point of incipient cavitation was observed to approach nearer to the hub-side apart from  $a_1$  point at the blade inlet. [The discontinuous change of cavitation characteristics like the above was taken up by Gongwer<sup>(5)</sup>.] Considering that this phenomenon was due to the change of flow conditions in the adjacent part of the impeller inlet, measurements of flow at the impeller inlet were conducted as follows, for the purpose of clarifying this phenomenon. Namely, a cylindrical 2-hole Pitot tube was placed at 35 mm apart from the impeller inlet at right angles to the shaft center-line, so that the change of velocity distribution at various capacities could be obtained. The outside diameter of Pitot tube was 9.5 mm. By the balance of pressure at the two measuring holes the direction of flow was obtained, as well as its static pressure, and the total pressure was measured by turning the tube<sup>(6)</sup>. (As to the Pitot tube used, correction was made by means of parallel jet flow, and the change in flow area at the suction pipe caused by the insertion was corrected also.) Nine measuring points were taken as shown in Fig.10. The fixing style is seen in Fig.9.

Fig.10 shows the relation between the capacity and the flow direction at each measuring point. The swirl angle  $\theta$  is the angle formed by the flow and the axial direction. As clearly shown in the Figure, when capacity was decreased to approxi-

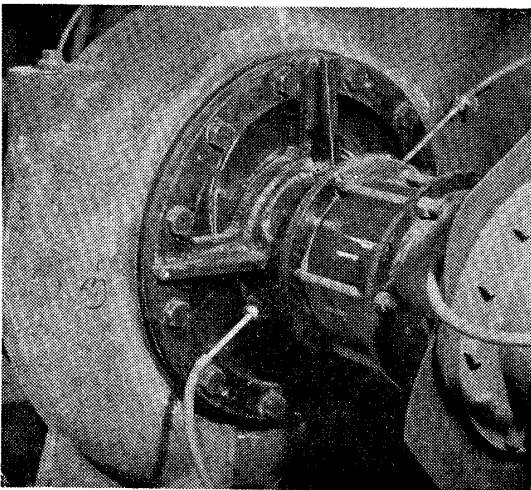


Fig. 9 Test pump with cylindrical Pitot tube

mately 45% of the normal, the flow suddenly started swirling towards circumferential direction, and near the pipe wall the swirl angle reached more than 90 deg. This fact shows that there might exist a back flow component. This swirling had a tendency to spread to the central part in accordance with the decrease in capacity. Velocity distributions obtained by the application of a cylindrical Pitot tube to such a three dimensional flow may not be accurate. However, velocity distributions obtained by the above method are as follows: Namely, in the range of capacity which was not accompanied by swirling, the flow showed uniform as shown in Fig.11 (a). On the contrary, in the range of capacity accompanied by swirling and back flow, axial velocity  $v_a$  was large near the hub and showed a back flow near the pipe wall, and circumferential velocity  $v_u$  increased radially forming a forced vortex as shown in Fig.11 (b). By this reason, it was found that the static pressure was low in the central part. It is presumed that the meridian flow pattern at the impeller inlet showed a flow from the hub toward radial direction owing to centrifugal force, and a part of flow directed against the shroud was turned to produce the backflow, as shown in Fig.12. These results show the same tendency as obtained by Peck's investigations<sup>(7)</sup>.

Referring to Fig.6, the capacity corresponding

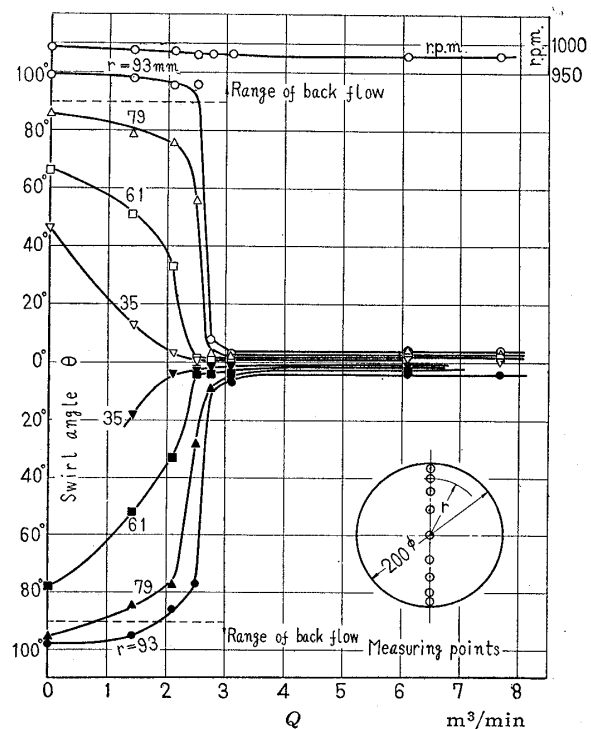


Fig. 10 Capacity versus swirl angle at impeller inlet (C-impeller)

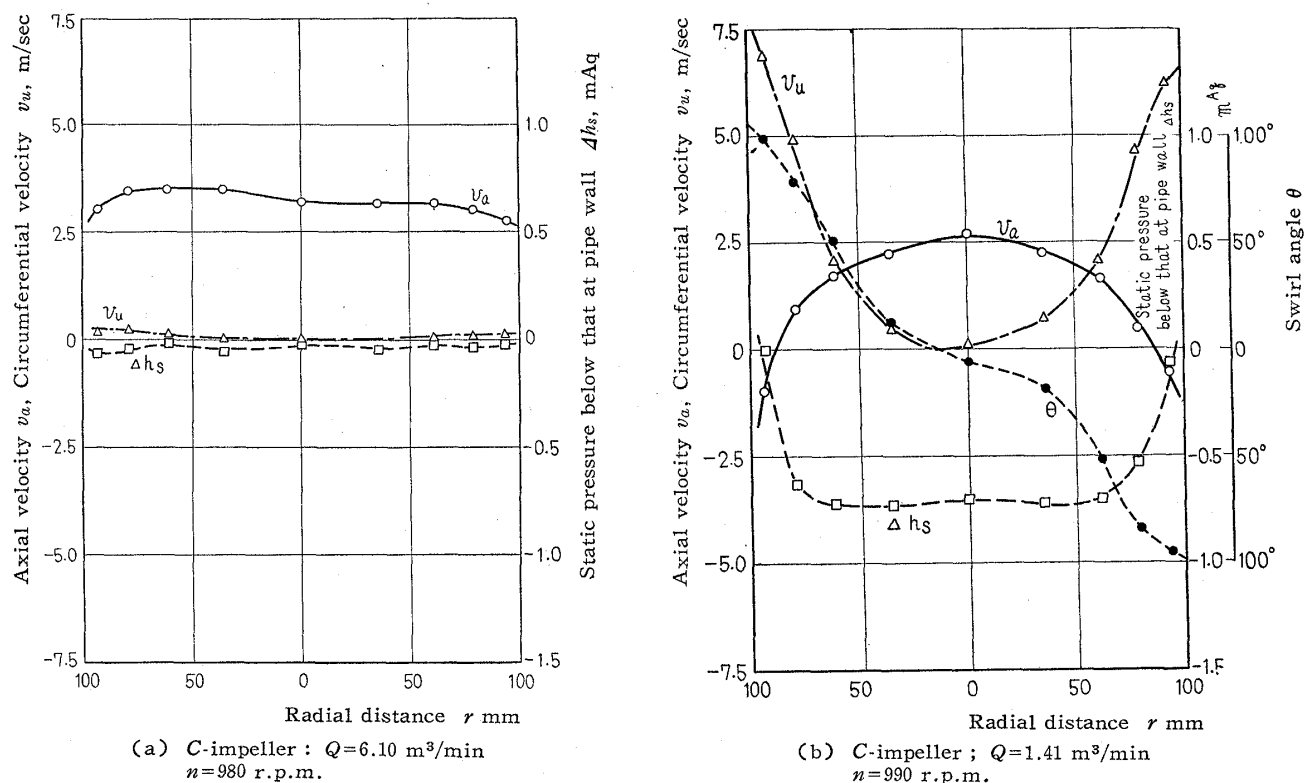


Fig. 11 Velocity and pressure distributions at impeller inlet

to the maximum NPSH at the incipient condition is approximately identical to that at which swirling starts in the flow at the impeller inlet (as mentioned above). When the capacity further decreases, the pressure becomes high in the adjacent part of the  $a_1$  point owing to the swirling and the high pressure water inside the impeller flowing back, and thus the cavitation is restrained. Furthermore, meridian velocity increases in the adjacent part of the hub where the relative velocity is small, at the same time  $\Delta\beta$  becoming small. Consequently it is explained that NPSH which accompanies incipient cavitation decreases together with the capacity. With the  $D$ -impeller, the capacity corresponding to the maximum value of  $H_{svi}$  was comparatively large, for it was more apt to cause swirling at the inlet than other impellers.

### 5. Aspects of cavitation and variation of pump performance

Photographic observation of cavitation appearing on the impeller having been conducted already<sup>(8)</sup>, we took up this matter again. Several cases of cavitation appearing during the tests taken by high speed photography are presented in Fig. 13. As shown in the photographs, the aspects of cavitation varied in accordance with the shape of impeller, capacity, and suction conditions. In the vicinity of normal capacity at  $\Delta\beta \doteq 0$ , cavitation

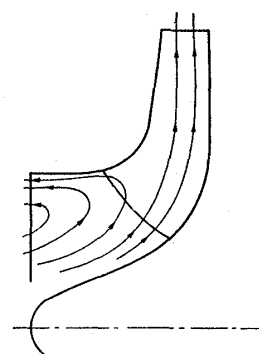


Fig. 12 Flow pattern at partial capacities

appeared on the front and back sides of the blade inlet along the front shroud as seen in Photo. 4, and this cavitation developed as shown in Photo. 5. Photo. 4 shows the condition just before the head drop. When a cavity was formed at the front side of the blade near the inlet along the shroud as shown in Photo. 5, the head showed the perpendicular drop. When the number of blades was few, cavitation was apt to develop in a longish style along the back side of the blade as seen in Photo. 6.

When the capacity was small, cavitation developed at the back of the blade inlet (see Photo. 1), and with a further decrease in the suction pressure a cavity was formed in front of the blade causing the head drop (see Photo. 2). In the

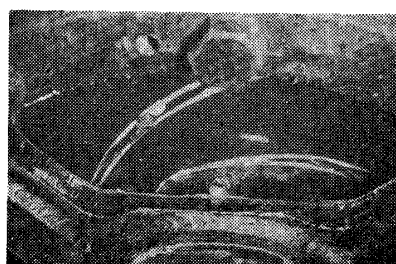


Photo. 1 C-impeller  
 $Q=4.15 \text{ m}^3/\text{min}$ ,  $H=16.17 \text{ m}$ ,  
 $H_{sv}=1.23 \text{ m}$ ,  $n=984 \text{ r.p.m.}$



Photo. 4 C-impeller  
 $Q=6.09 \text{ m}^3/\text{min}$ ,  $H=13.39 \text{ m}$ ,  
 $H_{sv}=1.59 \text{ m}$ ,  $n=980 \text{ r.p.m.}$

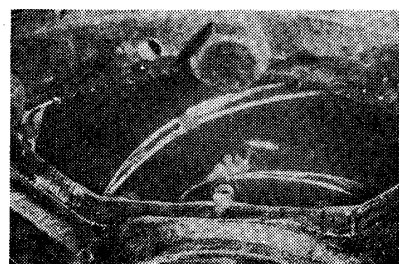


Photo. 7 C-impeller  
 $Q=7.25 \text{ m}^3/\text{min}$ ,  $H=11.03 \text{ m}$ ,  
 $H_{sv}=4.91 \text{ m}$ ,  $n=983 \text{ r.p.m.}$



Photo. 2 C-impeller  
 $Q=4.27 \text{ m}^3/\text{min}$ ,  $H=15.55 \text{ m}$ ,  
 $H_{sv}=0.82 \text{ m}$ ,  $n=984 \text{ r.p.m.}$

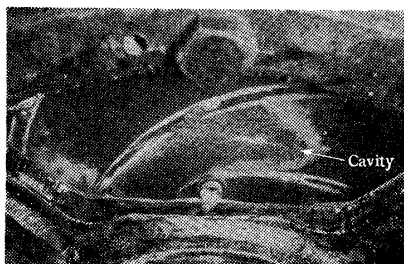


Photo. 5 C-impeller  
 $Q=6.17 \text{ m}^3/\text{min}$ ,  $H=12.21 \text{ m}$ ,  
 $H_{sv}=1.60 \text{ m}$ ,  $n=983 \text{ r.p.m.}$

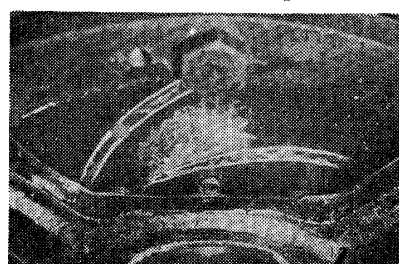


Photo. 8 A-impeller  
 $Q=7.50 \text{ m}^3/\text{min}$ ,  $H=8.61 \text{ m}$ ,  
 $H_{sv}=4.70 \text{ m}$ ,  $n=974 \text{ r.p.m.}$



Photo. 3 B-impeller  
 $Q=4.87 \text{ m}^3/\text{min}$ ,  $H=12.98 \text{ m}$ ,  
 $H_{sv}=1.28 \text{ m}$ ,  $n=983 \text{ r.p.m.}$



Photo. 6 B-impeller  
 $Q=6.33 \text{ m}^3/\text{min}$ ,  $H=11.41 \text{ m}$ ,  
 $H_{sv}=2.04 \text{ m}$ ,  $n=980 \text{ r.p.m.}$

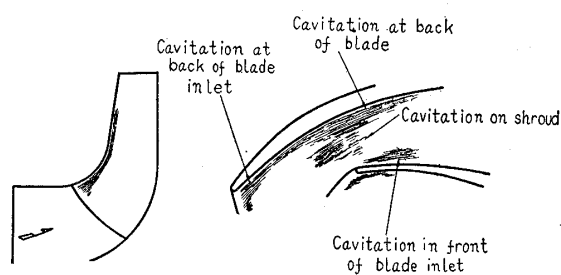


Photo. 9 D-impeller  
 $Q=7.35 \text{ m}^3/\text{min}$ ,  $H=11.06 \text{ m}$ ,  
 $H_{sv}=2.46 \text{ m}$ ,  $n=985 \text{ r.p.m.}$

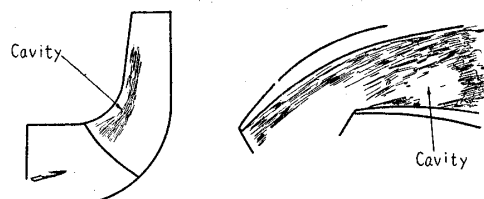
Fig. 13 Photographs of cavitation in impellers

case when the number of blades was few, a cavity appeared also at the back of the blade located at halfway of the flow passage (see Photo. 3). When the capacity was large, cavitation appeared at the front of the blade inlet (see Photo. 7), which easily developed to form a cavity along the shroud (see Photo. 8). It was possible to prevent forming of cavity at the front side of the blade inlet in order to check the head-drop by improving the design (see Photo. 9).

Cavitation first occurs locally at low pressure zone in the impeller and develops in accordance with the decrease of suction pressure. It is considered there are various pressure drops in the impeller<sup>(9)(10)</sup>. Namely, (1) Pressure drop on the tip of blade inlet, (2) that by the deflection of flow from axial to radial direction, (3) that by the pressure difference between the front and back sides of blade owing to the momentum which is applied to the flow by the blade motion, etc. It is considered that these factors combine with one



(a) Cavitation at incipient stage



(b) Developed cavitation

Fig. 14 Illustration of cavitation in impellers

another and make a complicated pressure distribution in the impeller.

Now, to give our explanation for Photo. 4, in Fig. 13, Fig. 14 (a) is presented. Cavitation at the front and back sides of the blade inlet tips is considered chiefly owing to the fact that increase in relative velocity is caused locally by the small radius of curvature at the inlet edge as mentioned in (1) above, which brings forth simultaneously the pressure drop. The cavitation on the shroud is considered due to generation of low pressure by the turning of a stream as mentioned in (2). When the blade inlet is located at a point on the shroud with a large curvature, pressure drop is doubled by (1) and (2), and a cavitation may occur easily. The cavitation at the back of the blade tends to develop in an elongated shape. This is owing to the low pressure at the back of the blade caused by the action mentioned in (3), which has been proved by other experimental results<sup>(11)(12)</sup>. Fig. 14 (b) is corresponding to Photo. 5 in Fig. 13, showing the developed cavity causing the head drop.

With regard to noise, though the cavitation at the front side of the blade at overcapacities often developed to a large cavity, its noise was not so great. On the other hand, when cavitation appeared at the back of the blade at partial capacities, it entailed a heavy impinging noise.

## 6. Comparison of pressure drop coefficients and suction specific speeds

Since the pressure drop in the impeller connected with the cavitation occurrence is caused by various factors as mentioned in the foregoing section, it is difficult to treat them separately from the experimental data obtained. Regarding the impellers reported here, we conducted a comparative study by representing the NPSH indicating each cavitation characteristics in the form of Formula

(2). First, the pressure drop coefficient at incipient cavitation  $\lambda_{wi}$  was obtained by Formula (2) by inserting the value of NPSH at the incipient cavitation, as plotted in Fig. 15. Representing the NPSH corresponding to the beginning of head drop as Formula (3), using the coefficient  $\lambda_{wd}$  corresponding to the same point, the variation of  $\lambda_{wd}$  was plotted in Fig. 16.

$$H_{svd} = \frac{c_1^2}{2g} + \lambda_{wd} \frac{w_1^2}{2g} \quad \dots\dots\dots (3)$$

In both Figs. 15 and 16, capacity was represented in terms of flow rate coefficient  $\phi$  (ratio of average axial velocity at the impeller inlet  $v_s$  to peripheral velocity  $u_s$  at the impeller eye), the value of  $\phi$  which corresponded to  $\Delta\beta=0$  being denoted as  $\phi_0$  for each impeller. The coefficient  $\lambda_{wi}$ , which indicates the incipient cavitation, shows minimum near the point of  $\Delta\beta=0$ , and indicates the remarkable effect by  $\Delta\beta$  on both sides of  $\phi_0$ . Further, this coefficient  $\lambda_{wi}$  reaches a peak at a partial capacity at which  $H_{svi}$  reached also its peak. The peak value of this  $\lambda_{wi}$  is largest with the C-impeller and is smallest with the D-impeller.

On the other hand,  $\lambda_{wd}$  corresponding to the head drop shows a remarkable increase as the capacity becomes larger than at  $\Delta\beta=0$ , indicating that when the value of  $\Delta\beta$  passes from positive to negative the flow at the blade inlet produces a condition in which a cavity is apt to appear<sup>(5)</sup>. When the capacity becomes less than the design point  $\lambda_{wd}$  decreases slowly and under partial capacities it approaches to an approximately constant value. Under the capacity where  $\Delta\beta=0$ , each impeller shows approximately  $\lambda_{wd}=0.2$ . The inclination of  $\lambda_{wd}$  at overcapacities is smallest with the D-impeller, followed by the B-impeller. On the other hand, NPSH at the point of head drop can be represented by the following Formula considering the absolute velocity  $c_1$  at the blade inlet:

$$H_{svd} = \lambda_{cd} \frac{c_1^2}{2g} \quad \dots\dots\dots (4)$$

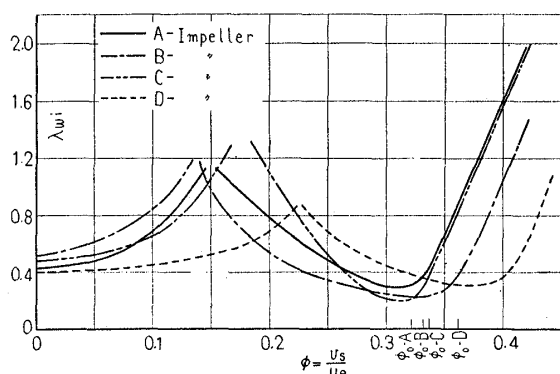


Fig. 15 Capacity versus coefficient  $\lambda_{wi}$  at incipient condition

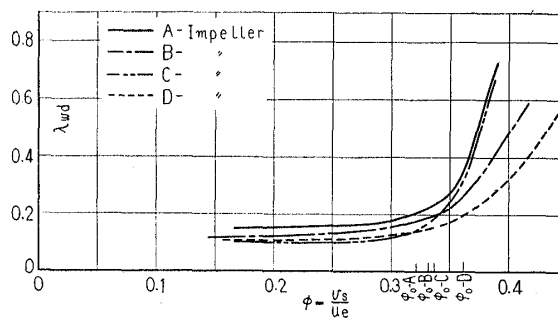


Fig. 16 Capacity versus coefficient  $\lambda_{wd}$  at beginning of head drop

The variation of the coefficient  $\lambda_{cd}$  obtained from Formula (4) is shown in Fig. 17;  $\lambda_{cd}$  shows an increase on both sides of  $\Delta\beta=0$ , which fact testifies to the influence of  $\Delta\beta$ .

Now, the limits concerning the incipient cavitation and the head drop point are shown in Figs. 18 and 19 in terms of the suction specific speed  $S$  ( $\text{m}^3/\text{min}$ ,  $\text{m}$ ,  $\text{r.p.m.}$ ) which is convenient in checking the suction characteristics from the operating specifications. The value of  $S_i$  indicating the incipient stage of cavitation is about 1200 in the adjacent range of  $\Delta\beta=0$ , but with the C-impeller  $S_i$  is as high as 1480. With the B and D-impellers, the fluctuation of  $S_i$  is comparatively small. The value  $S_d$  which shows the head drop point is about 1400 at  $\Delta\beta=0$ , and the variation versus capacity is most favourable with the D-impeller, followed by the B-impeller.

## 7. Conclusions

Experiments on cavitation in a centrifugal pump were conducted with impellers having three dimensional blades, whose results were stated as above. The principal points are as follows:

(1) Variations of NPSH over wide ranges of capacity at the condition of incipient cavitation at the blade inlet were obtained by observation with strobo-light. The performance deterioration due to cavitation was also measured.

(2) The NPSH at the incipient stage for each impeller showed minimum at or near the normal capacity and increased at the both sides owing to the influence of the angle of incidence, and it was found to take a certain maximum value at a partial capacity.

(3) The discontinuous change of this NPSH under the partial capacity was explained by the measurements of flow at the impeller inlet, through which it was clarified that the flow pattern at partial capacities accompanying swirling and back flow was the cause for such NPSH fluctuations.

(4) Cavitation aspects were observed actually and by photography to clarify the relation with the performance variation. The correlation of cavitation occurrence to various pressure depressions in the impeller was discussed.

(5) By using the pressure drop coefficients as well as the suction specific speed, suction characteristics of each impeller were represented graphically with regard to capacity with a view to applying to the practical fields. As the result of comparing four kinds of the impeller, with the B-impeller which had a fewer number of blades the pressure drop coefficients at the incipient cavitation and at the performance deterioration

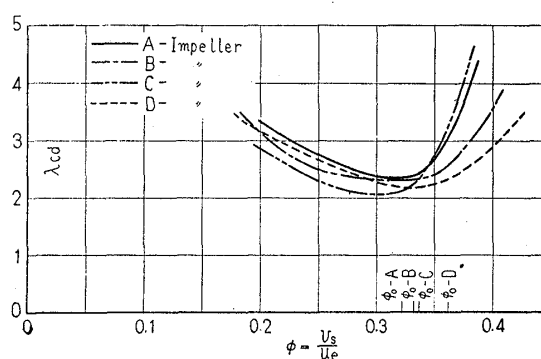


Fig. 17 Capacity versus coefficient  $\lambda_{cd}$  at beginning of head drop

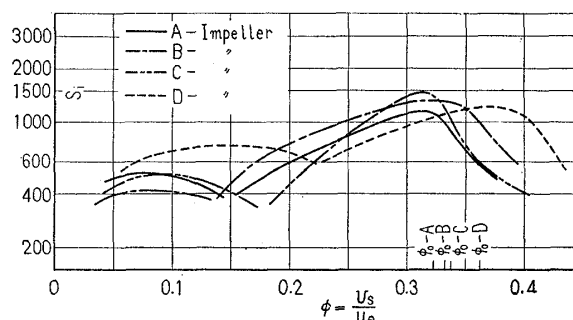


Fig. 18 Capacity versus suction specific speed at incipient condition

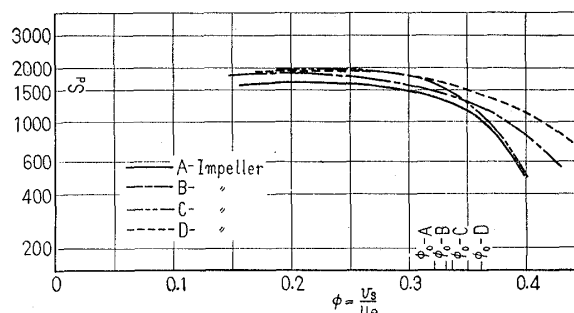


Fig. 19 Capacity versus suction specific speed at beginning of head drop

were smaller than with the A-impeller. The C-impeller which had smaller thickness at the inlet tips showed a good performance in the vicinity of the normal capacity, but the maximum value of NPSH at the incipient condition under the partial capacity was large. With the D-impeller this maximum value was small and the suction performance was superior even under overcapacities.

In accordance with the speed up of pumps, elimination of cavitation is demanded seriously in manufacturing pumps as well as in their operation. It would be very fortunate for us if the above mentioned study may contribute to meeting the demand.

## References

- (1) C Pfeleiderer: *VDI-Z*, Bd. 92, Nr. 23 (1950), S. 629.
- (2) G.F. Wislicenus: *Trans. ASME*, Vol. 78, No. 8

- (1956), p. 1707.
- (3) H. Cardinal von Widdern: *Escher-Wyss Mitteilungen*, Januar-Marz (1936), S. 14.
- (4) R. Dziallas: *VDI-Z*, Bd. 89, Nr. 3/4, (1945), S. 41.
- (5) A. Gongwer: *Trans. ASME*, Vol. 63, No. 1 (1941), p. 29.
- (6) R.C. Binder and R.T. Knapp: *Trans. ASME*, Vol. 58, (1936), p. 649.
- (7) J.F. Peck: *Proc. Instn. Mech. Engrs.*, Vol. 164, No. 1 (1951), p. 1.
- (8) M. Yamamasu: *Jour. Japan Soc. Mech. Engrs.*, Vol. 60, No. 459 (1957), p. 416.
- (9) A.J. Stepanoff: *Centrifugal & Axial Flow Pumps*, (1948), Chapt. 12, John Wiley & Sons.
- (10) C. Pfeleiderer: *Kreiselpumpen für Flüssigkeiten und Gase* (1955), Julius Springer.
- (11) A.J. Acosta: *Trans. ASME*, Vol. 79, No. 8 (1957), p. 182.
- (12) G. Kamimoto and I. Matsuoka: *Trans. Japan Soc. Mech. Engrs.*, Vol. 22, No. 113 (1956), p. 55.

621.67-154:532.517

## Flow in Axial Blade\*

By Takefumi IKUI\*\*

The flow behaviours of the flow field in a impeller and guide vane of axial blower have been observed using the technique of visualization by silk tufts. When the stall zone is limited to the tip region only, the surging zone on the  $\psi$ - $\phi$  characteristics does not appear clearly. Therefore, if the suction or delivery concentric rings have the effect to prevent the stall zone from extending toward the section within geometrical mean radius, the stall characteristics of an axial machine will be improved.

In the stationary guide vane of an axial blower, the blade characteristics are better than those of other section, owing to the flow in the boundary layer from tip to root caused by a secondary flow in the curved channel.

### Introduction

In this paper, the author describes the flow behaviour in an axial impeller and guide vane of a retarded flow free from cavitation. It is desirable that cavitation does not occur in the nominal point of hydraulic machine. And in the cavitationless flow condition, a fluid flow in the axial pump is same as that in the axial blower if the compressibility of air is neglected, because Reynolds number and the blade design theory are nearly the same between pump and blower.

The author advises use of air to observe the flow behaviours in the impeller, guide vane and other parts of hydraulic pump, because air is more convenient to treat, to photograph and to make fine observation than water. Therefore in the following description, research results on one stage axial blower are stated. Further, he describes the flow condition in an axial impeller and guide vane at running state but not the flow behaviour in a two-dimensional cascade.

### Nomenclature

The following nomenclature is used in the paper.

\* Received 3rd February, 1959.

\*\* Professor of Kyushu University, Research Institute of Science and Industry, Fukuoka.

$c_a$  : axial velocity

$c_L$  : lift coefficient

$l$  : chord length

$r$  : radius

$t$  : pitch of blade

$u$  : peripheral velocity

$\alpha$  : angle of attack

$\phi$  : flow coefficient  $c_a/u$

$\psi$  : pressure coefficient,  $P_t / \frac{\gamma}{2g} u_t^2$

$\gamma$  : specific weight of fluid

subscript  $t$  : blade tip

Other symbols are illustrated in the Figures.

### 1. Flow in axial impeller

The peripheral velocity of one stage axial blower is at most about twice or thrice as large as that of one stage axial pump. But Reynolds number of impellers of axial blower and pump at running state are almost of same order which is limited to about  $10^4 \sim 10^6$ . The work to be reported here involves the investigations of the detailed visualized flow behaviours in the different axial blades. Fig.1 is the dimensionless characteristics of one stage axial blower of axial inlet type with 320 mm diameter and 0.5 hub ratio.

Fig.2 is the behaviours of a flow in the